

# DeSAM: Decoupling Segment Anything Model for Generalizable Medical Image Segmentation

Yifan Gao<sup>1,2</sup>, Wei Xia<sup>2</sup>, Dingdu Hu<sup>1,2</sup>, and Xin Gao<sup>2</sup>✉

<sup>1</sup> School of Biomedical Engineering, Division of Life Science and Medicine, University of Science and Technology of China, Hefei, China

<sup>2</sup> Suzhou Institute of Biomedical Engineering and Technology, Chinese Academy of Sciences, Suzhou, China

yifangao@mail.ustc.edu.cn, hudingdu@mail.ustc.edu.cn  
xiaw@sibet.ac.cn, xingaosam@163.com

**Abstract.** Deep learning based automatic medical image segmentation models often suffer from domain shift, where the models trained on a source domain do not generalize well to other unseen domains. As a vision foundation model with powerful generalization capabilities, Segment Anything Model (SAM) shows potential for improving the cross-domain robustness of medical image segmentation. However, SAM and its fine-tuned models performed significantly worse in fully automatic mode compared to when given manual prompts. Upon further investigation, we discovered that the degradation in performance was related to the coupling effect of poor prompts and mask segmentation. In fully automatic mode, the presence of inevitable poor prompts (such as points outside the mask or boxes significantly larger than the mask) can significantly mislead mask generation. To address the coupling effect, we propose the decoupling SAM (DeSAM). DeSAM modifies SAM’s mask decoder to decouple mask generation and prompt embeddings while leveraging pre-trained weights. We conducted experiments on publicly available prostate cross-site datasets. The results show that DeSAM improves dice score by an average of 8.96% (from 70.06% to 79.02%) compared to previous state-of-the-art domain generalization method. Moreover, DeSAM can be trained on personal devices with entry-level GPU since our approach does not rely on tuning the heavyweight image encoder. The code is publicly available at <https://github.com/yifangao112/DeSAM>.

**Keywords:** Segment Anything Model · Medical Image Segmentation · Single-source Domain Generalization.

## 1 Introduction

Deep learning models achieve remarkable performance in medical image segmentation when trained and evaluated on data from the same domain [1–3]. However, the generalizability of deep models may be poor to unseen out-of-domain data, which prevents the use of models in clinical settings. To mitigate

the performance degradation caused by domain shifting, previous attempts focus on unsupervised domain adaptation [4] and multi-source domain generalization [5]. However, unsupervised domain adaptation and multi-source domain generalization rely on training data from the target domain or from multiple source domains. Such requirements may not hold due to cost and privacy issues, making it difficult for real-world clinical applications.

A more practical but challenging method is single-source domain generalization: using training data from only one source domain to train deep learning models robust to unseen data. The main solutions include input space-based and feature-based data augmentation [6]. Yet there are some limitations with solutions: input space-based augmentation requires expertise to design the augmentation function, and feature-based augmentation usually requires complex adversarial training [7].

Compared to the above approaches, directly migrating models based on large datasets to medical image segmentation to improve generalization is an attractive approach. Some early work utilized pre-trained models on natural or medical images and achieved good performance [8,9]. However, due to the small capacity of the pre-trained models, the cross-domain generalizability of the deep models was not effectively improved.

Recently, vision foundation models have made great progress in image segmentation [10–12]. Segment Anything Model (SAM) [10], trained on more than 1 billion masks, has achieved unprecedented generalization capabilities on a variety of natural images. Some work shows that adapting SAM to medical image segmentation also shows good results. These advances demonstrate the promise of training a powerful segmentation model with generalizability using pre-trained SAM without the need to design a complex pipeline of data enhancements. There were two main approaches methods adapting SAM to medical image segmentation, and the limitations of the two main approaches were: 1) the method freezing the image encoder and prompt encoder of SAM and fine-tune only the mask decoder usually yields suboptimal results, 2) the method training the image encoder using adaption [13, 14] or visual prompt [15] techniques improves the performance of the model in a specific domain. However, since image embeddings cannot be computed in advance, training such a model requires high GPU memory consumption. In addition, these fine-tuning methods still require the use of manually given boxes or points, making it difficult to achieve fully automated medical image segmentation.

There are two ways to achieve automatic segmentation directly through SAM. One is to use grid points as prompt, which we call *grid points mode*, and the other is to use boxes of the same size as the image for the prompt, which we call *whole box mode*. However, even after complete fine-tuning, the fully automated SAM tends to produce a large number of false positive masks, and the performance is far inferior to meet the clinical requirements. Therefore, achieving high-performance fully automated medical image segmentation based on SAM is an urgent problem to be solved. We argue that the poor performance of fully automated SAM in medical image segmentation can be attributed to a mechanism,

namely **the coupling effect**: image embeddings and prompt tokens interacted in the cross-attention transformer layer of SAM mask decoder, which makes the final output mask highly dependent on the prompt. Therefore, even after fine-tuning, the model still tends to be more sensitive to wrong prompts (i.e., points that are not in the mask, or the boxes that are significantly larger than the mask).

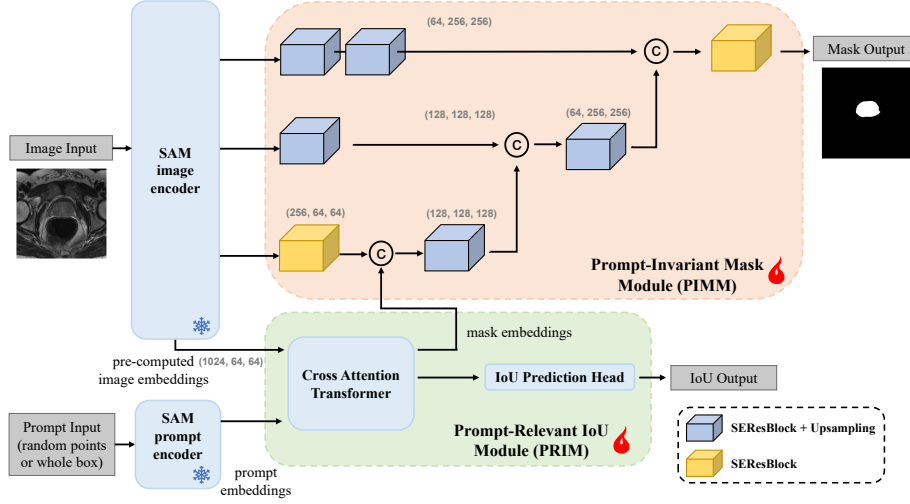


**Fig. 1.** Overview of the proposed DeSAM. The DeSAM consists of the image and prompt encoders of SAM, a Prompt-Invariant Mask Module (PIMM), and a Prompt-Relevant IoU Module (PRIM). The image encoder are used to compute the image embeddings before training. The prompt encoder is frozen during training. The PIMM consists of a cross-attention transformer and an IoU prediction head, and it utilizes the image and prompt embeddings to generate mask embeddings and IoU score. The PRIM contains multiple SEResBlocks and upsampling operations, and it integrates the mask embeddings and image embeddings to generate the mask.

To address this issue, we propose Decoupling Segment Anything Model (DeSAM) in this work, a novel architecture for fully automated medical image segmentation based on SAM. We decouple the mask decoder of SAM into two subtasks: 1) prompt-relevant IoU regression, 2) prompt-invariant mask learning. Specifically, we design two new modules and added to the fully automated SAM. The first one is the prompt-relevant IoU module (PRIM), which predicts IoU scores based on given prompt and generates mask embeddings. The second one is the prompt-invariant mask module (PIMM), which fused the image embeddings from the image encoder with the mask embeddings from PRIM to generate the mask. DeSAM minimizes the performance degradation caused by wrong prompts in the segment-everything mode. In addition, DeSAM does not need to train image encoder, which means that image embeddings can be com-

puted before training to significantly reduce the requirement of GPU memory. The full-size SAM model (ViT-H) based DeSAM can run on an entry-level GPU, which is significantly more efficient than the previous encoder-based fine-tuning methods. Extensive experiments on publicly available prostate datasets show that the DeSAM improves the robustness of fully automated prostate segmentation against distribution variations across different sites.

## 2 Related Work

### 2.1 Single-source domain generalization

Given training data from only one domain and generalizing to an unseen domain, single-source domain generalization is more challenging since there is less diversity in training domains. Thus, the mainstream solution to this problem is to generate novel domains using data argumentation techniques to increase the diversity and informativeness of training data. Several methods designed different generation strategies for single-source domain generalization in computer vision tasks. Chen et al. [16] augment data with the random bias field, the common image artifact in clinical MR images. RandConv [17] uses random convolutions for data augmentation. MixStyle adopts a combination of the style information of randomly-selected instances of different domains. Maxstyle [7] expands the domain space with additional noise and the worst-case composition. Ouyang et al. [18] propose a simple causality-inspired data augmentation method that greatly improves the cross-domain robustness of deep models. Unlike previous methods, DeSAM enhances the generalization ability of deep models without a complex pipeline for data argumentation, making it more competitive in practical applications.

### 2.2 Segment Anything Model

The remarkable extension ability of Transformer makes it possible to construct large-scale models with billions of parameters. SAM was the first proposed foundation model for image segmentation and has been applied to various computer vision applications [15, 19–30]. Intrigued by its unprecedented performance in natural image segmentation, considerable efforts have been made on its extended applications in medical image [31–43]. In particular, some work attempts to adapt SAM to medical image segmentation, including fine-tuning mask decoder and image encoder [13, 14, 44, 45]. Compared with these methods, our proposed DeSAM reaches balance between performance and efficiency and gains satisfactory results in fully automated segmentation.

## 3 Decoupling Segment Anything Model

### 3.1 Architecture

The overview of DeSAM is illustrated in Fig. 1. DeSAM contains three main components, the encoder, the Prompt-Invariant Mask Module (PIMM), and the

Prompt-Relevant IoU Module (PRIM). These components are described in detail in this section.

**DeSAM Encoder** In the DeSAM encoder, we use a pre-trained model ViT-H of SAM and freeze the image and prompt encoders during training. In particular, we do not make any tuning to the image encoder so that the image embeddings can be precomputed before the training stage. Therefore, the DeSAM training process does not require loading the image encoder. This makes our approach highly GPU efficient.

**Prompt-Relevant IoU Module (PRIM)** The PRIM has a similar structure to the mask decoder of SAM, which includes a cross-attention transformer layer and an IoU prediction head. However, to decouple the prompt and the output mask, we only discard the mask prediction head and extract mask embeddings from the cross-attention transformer layer.

**Prompt-Invariant Mask Module (PIMM)** Inspired by the architecture of U-Net [46] and UNETR [47], we adopt the classical encoder-decoder structure. First, we extract the image embedding from the global attention layer  $i$  of the image encoder. Specifically, in the image encoder ViT-H of SAM, the image embeddings with shape of  $1024 \times 64 \times 64$  are extracted from the global attention layer  $i = (8, 16, 24)$ . Secondly, we pass the image embeddings to different numbers of squeeze and excitation residual blocks (SEResBlock) and upsampling operations. Finally, we fuse the image embeddings by skipping connections. In addition, we merge the mask embeddings of PRIM and the bottleneck embeddings of PIMM to utilize the pre-training weights and ensure the gradient flow of PIMM and PRIM during training.

### 3.2 Training strategies

During training, we load the pre-trained weights of SAM, freeze the image and prompt encoders, and fine-tune the layers within PIMM and PRIM. Since the automatic segmentation includes the grid points mode and the whole box mode, we adopt two different strategies to train the proposed model. In the grid points mode, we randomly generate points within and outside the ground truth mask in a 1:1 ratio. Mask generation is supervised by dice loss  $L_{dice}$  and cross-entropy loss  $L_{ce}$ . IoU is supervised by mean square error loss  $L_{mse}$ . The total loss is:

$$L_{points} = \lambda_1 L_{dice} + \lambda_2 L_{ce} + \lambda_3 L_{mse} \quad (1)$$

The loss weight  $\lambda_1$ ,  $\lambda_2$ ,  $\lambda_3$  are 1, 1, and 10. In the whole box mode, since the ground truth mask must be inside the box, we only supervise the mask generation:

$$L_{box} = L_{dice} + L_{ce} \quad (2)$$

**Table 1.** Quantitative comparison of our DeSAM and state-of-the-art single-source domain generalization methods. The best performance is indicated by bolded fonts, and the second-best results is underlined.

Method	A to Rest	B to Rest	C to Rest	D to Rest	E to Rest	F to Rest	Overall
Upper bound [53]	85.38	83.68	82.15	85.21	87.04	84.29	84.63
Baseline [53]	63.73	61.21	27.41	34.36	44.10	61.70	48.75
AdvNoise [51]	72.15	63.26	30.81	40.12	48.07	60.12	52.42
AdvBias [16]	77.45	62.12	51.09	70.20	51.12	50.69	60.45
RandConv [17]	75.52	57.23	44.21	61.27	49.98	54.21	57.07
MixStyle [52]	73.04	59.29	43.00	62.17	53.12	50.03	56.78
MaxStyle [7]	81.25	70.27	62.09	58.18	70.04	67.77	68.27
CSDG [18]	80.72	68.00	59.78	72.40	68.67	70.78	70.06
MedSAM [44]	72.32	73.31	61.53	64.46	68.89	61.39	66.98
DeSAM (whole box)	<u>82.30</u>	<u>78.06</u>	<b>66.65</b>	<u>82.87</u>	<u>77.58</u>	<u>79.05</u>	<u>77.75</u>
DeSAM (grid points)	<b>82.80</b>	<b>80.61</b>	<u>64.77</u>	<b>83.41</b>	<b>80.36</b>	<b>82.17</b>	<b>79.02</b>
Impro. over baseline	+19.07	+19.40	+37.36	+49.05	+36.26	+20.47	+30.27

## 4 Results and Discussion

### 4.1 Dataset and implementation details

To evaluate the performance of the proposed DeSAM, we created a multi-site prostate segmentation dataset containing three publicly available datasets from six different clinical sites. The cross-domain images were collected from three independent public datasets containing NCI-ISBI-2013 [48], I2CVB [49], and PROMISE12 [50]. We took the same pre-processing methods as MaxStyle [7]. More specifically, all images were preprocessed with a spatial resolution of  $0.625 \times 0.625 \times 3.6 \text{ mm}^3$  and an image size of  $288 \times 288$ , with an intensity range between 0 and 1. In each experiment, we split the data from one site into a training set and an in-domain validation set in a 9:1 ratio. The best-performing model in the in-domain validation set was then tested for cross-site robustness on the other five sites. We use the dice score as the evaluation metric to measure the quality of the predicted masks.

The image embeddings were precomputed before training using the ViT-H model as image encoder. We set the number of points for the grid points mode to  $9 \times 9$ . We used the learning rate =  $1e-4$  and batch size = 8 for network optimization and applied learning rate decay. The network was trained for 50 epochs for the prostate dataset to ensure convergence. We performed the experiments on a single RTX 3060 12GB. During training, the video memory usage was approximately 7.8 GB. The total time for training varied between 1.2 hours and 2.7 hours, depending on the number of training images at each site. We conducted the system-level comparison of our method with the upper bound (fully supervised on the seen domain), baseline (no domain generalization), MedSAM [44], and other state-of-the-art single-source domain generalization methods, including 1) adversarial noise (AdvNoise) [51]; 2) adversarial bias field (AdvBias) [16];

3) RandConv [17]; 4) MixStyle [52]; 5) MaxStyle [7]; and 6) causality-inspired domain generalization (CSDG) [18]. Upper bound and baseline experiments were implemented using nnU-Net [53], MedSAM was implemented in the whole box mode, and all other comparison methods used their recommended settings.

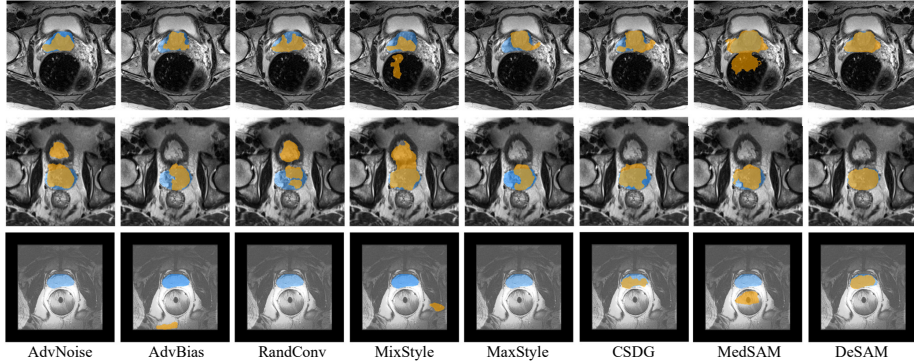


**Fig. 2.** Visual comparison of different methods for cross-site prostate segmentation. Orange and blue regions denote the predicted mask and ground truth mask, respectively.

## 4.2 Comparison with state-of-the-art methods

As summarized in Table 1, DeSAM consistently achieves impressive advances in the segmentation performance on unseen domains for the prostate cross-site dataset. Compared to the baseline, DeSAM achieved significant improvements, particularly in domain D where it improved the dice score from 34.36% to 83.41%, an increase of 49.05%. Most generalization methods achieved remarkable performance in specific domains but failed in others. In comparison, DeSAM achieves state-of-the-art performance among six domains, demonstrating its strong generalization ability. It is important to note that the comparison between MedSAM and DeSAM (whole box) highlights the contribution of our proposed decoupling strategy. The results show that our approach improves the average dice score by 10.77% (from 66.98% to 77.75%) by reducing the impact of poor prompts on segmentation quality, demonstrating a significant improvement from MedSAM to DeSAM. Fig. 2 shows a visual comparison between the different methods of prostate segmentation. In contrast, our DeSAM achieves better results than the others, with no false positives in the background and segmentation boundaries very close to the ground truth.

## 4.3 Ablation studies

We performed a series of ablation experiments to validate the key design choices in our DeSAM. If not specified, the grid points mode with  $9 \times 9$  points are used

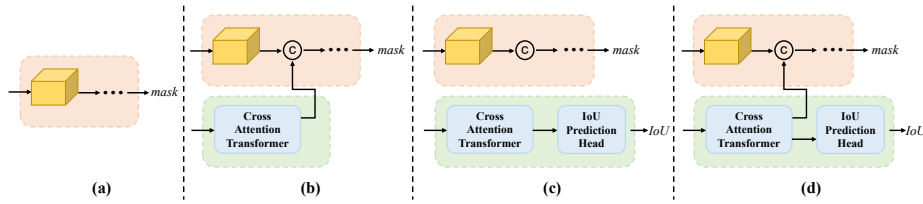


**Fig. 3.** Design choices of the decoder. (a) Generating a mask by directly using the image embedding from the encoder (PIMM only). (b) PIMM and PRIM without IoU prediction head. (c) PIMM and PRIM without mask embedding fusion. (d) Our proposed DeSAM.

**Table 2.** Quantitative results of our ablation experiments. The best performance is indicated by bolded fonts.

Method	A to Rest	B to Rest	C to Rest	D to Rest	E to Rest	F to Rest	Overall
PIMM only	79.09	74.96	54.19	80.11	77.22	77.53	73.85
PIMM + PRIM w/o IoU prediction head	76.74	76.61	58.94	80.45	78.39	79.56	75.12
PIMM + PRIM w/o mask embedding fusion	79.52	78.37	59.59	82.65	80.16	74.58	75.81
DeSAM	<b>82.80</b>	<b>80.61</b>	<b>64.77</b>	<b>83.41</b>	<b>80.36</b>	<b>82.17</b>	<b>79.02</b>

for prediction by default setting. For the ablation study, we compared our DeSAM with three variants: (a) Generating a mask by directly using the image embedding from the encoder (PIMM only). (b) PIMM and PRIM without IoU prediction head. (c) PIMM and PRIM without mask embedding fusion. Fig. 3 shows the difference between the three variants and DeSAM. The results in Table 2 show that the performance of our model is improved by gradually adding these components.

To investigate the robustness of our method in the grid points mode, we experimented with different numbers of grid points, i.e., 1, 5, 9, 11, 15, 21, and 25, respectively. Table 3 reports the quantitative results. The results show that there is no degradation in the performance of the model as the number of grid points increases, indicating the effectiveness of our method in avoiding false positive masks affected by poor prompts in the grid points mode.

## 5 Conclusion

We introduce DeSAM, a powerful network architecture for single-source domain generalization in medical image segmentation. It decouples mask generation from prompt and takes advantage of the pre-trained weights of SAM. DeSAM motivates the decoder to learn prompt-invariant features from robust image embeddings. Moreover, DeSAM has strong ability to resist unseen distribution changes by fusing image embeddings at multiple scales. We validated the performance of DeSAM on the prostrate cross-site dataset, demonstrating that the proposed method outperforms other state-of-the-art methods.

**Table 3.** Quantitative results of different number of points.

Grid Points	A to Rest	B to Rest	C to Rest	D to Rest	E to Rest	F to Rest	Overall
1	82.00	76.33	62.28	83.40	80.31	79.30	77.27
5	82.33	77.72	64.66	83.40	80.32	80.65	78.18
9	82.80	80.61	64.77	83.41	80.36	82.17	79.02
11	82.81	80.70	64.74	83.43	80.34	82.24	79.04
15	82.81	80.68	64.76	83.45	80.29	82.25	79.04
21	82.81	80.62	64.75	83.44	80.34	82.20	79.03
25	82.82	80.64	64.75	83.40	80.33	82.22	79.03

It is worth mentioning that DeSAM is computationally efficient compared to other methods that fine-tune the encoder. Our method can be trained on an entry-level GPU by precomputing the image embedding. Although further improvements in performance could be achieved by loading the image encoder to apply regular image augmentation, our DeSAM has already achieved satisfactory results. Beyond that, integrating DeSAM with other domain generalization methods would be an exciting direction to explore. We hope that DeSAM will enable more generalizable, powerful, and computationally efficient medical image segmentation.

## References

1. Yifan Gao, Yin Dai, Fayu Liu, Weibing Chen, and Lifu Shi. An anatomy-aware framework for automatic segmentation of parotid tumor from multimodal mri. *Computers in Biology and Medicine*, page 107000, 2023.
2. Dingdu Hu, Junming Jian, Yongai Li, and Xin Gao. Deep learning-based segmentation of epithelial ovarian cancer on t2-weighted mr images. *Quantitative Imaging in Medicine and Surgery*, in press, 2022.
3. Xingyu Zhao, Peiyi Xie, Mengmeng Wang, Wenru Li, Perry J Pickhardt, Wei Xia, Fei Xiong, Rui Zhang, Yao Xie, Junming Jian, et al. Deep learning-based fully automated detection and segmentation of lymph nodes on multiparametric-mri for rectal cancer: A multicentre study. *EBioMedicine*, 56:102780, 2020.
4. Yaroslav Ganin and Victor Lempitsky. Unsupervised domain adaptation by back-propagation. In *International conference on machine learning*, pages 1180–1189. PMLR, 2015.
5. Krikamol Muandet, David Balduzzi, and Bernhard Schölkopf. Domain generalization via invariant feature representation. In *International conference on machine learning*, pages 10–18. PMLR, 2013.
6. Hao Guan and Mingxia Liu. Domain adaptation for medical image analysis: a survey. *IEEE Transactions on Biomedical Engineering*, 69(3):1173–1185, 2021.
7. Chen Chen, Zeju Li, Cheng Ouyang, Matthew Sinclair, Wenjia Bai, and Daniel Rueckert. Maxstyle: Adversarial style composition for robust medical image segmentation. In *International Conference on Medical Image Computing and Computer-Assisted Intervention*, pages 151–161. Springer, 2022.
8. Sihong Chen, Kai Ma, and Yefeng Zheng. Med3d: Transfer learning for 3d medical image analysis. *arXiv preprint arXiv:1904.00625*, 2019.

9. Zongwei Zhou, Vatsal Sodha, Jiaxuan Pang, Michael B Gotway, and Jianming Liang. Models genesis. *Medical image analysis*, 67:101840, 2021.
10. Alexander Kirillov, Eric Mintun, Nikhila Ravi, Hanzi Mao, Chloe Rolland, Laura Gustafson, Tete Xiao, Spencer Whitehead, Alexander C Berg, Wan-Yen Lo, et al. Segment anything. *arXiv preprint arXiv:2304.02643*, 2023.
11. Xueyan Zou, Jianwei Yang, Hao Zhang, Feng Li, Linjie Li, Jianfeng Gao, and Yong Jae Lee. Segment everything everywhere all at once. *arXiv preprint arXiv:2304.06718*, 2023.
12. Xinlong Wang, Xiaosong Zhang, Yue Cao, Wen Wang, Chunhua Shen, and Tiejun Huang. Seggpt: Segmenting everything in context. *arXiv preprint arXiv:2304.03284*, 2023.
13. Junde Wu, Rao Fu, Huihui Fang, Yuanpei Liu, Zhaowei Wang, Yanwu Xu, Yueming Jin, and Tal Arbel. Medical sam adapter: Adapting segment anything model for medical image segmentation. *arXiv preprint arXiv:2304.12620*, 2023.
14. Kaidong Zhang and Dong Liu. Customized segment anything model for medical image segmentation. *arXiv preprint arXiv:2304.13785*, 2023.
15. Tianrun Chen, Lanyun Zhu, Chaotao Ding, Runlong Cao, Shangzhan Zhang, Yan Wang, Zejian Li, Lingyun Sun, Papa Mao, and Ying Zang. Sam fails to segment anything?—sam-adapter: Adapting sam in underperformed scenes: Camouflage, shadow, and more. *arXiv preprint arXiv:2304.09148*, 2023.
16. Chen Chen, Chen Qin, Huaqi Qiu, Cheng Ouyang, Shuo Wang, Liang Chen, Giacomo Tarroni, Wenjia Bai, and Daniel Rueckert. Realistic adversarial data augmentation for mr image segmentation. In *International Conference on Medical Image Computing and Computer-Assisted Intervention*, pages 667–677. Springer, 2020.
17. Zhenlin Xu, Deyi Liu, Junlin Yang, Colin Raffel, and Marc Niethammer. Robust and generalizable visual representation learning via random convolutions. In *International Conference on Learning Representations*, 2021.
18. Cheng Ouyang, Chen Chen, Surui Li, Zeju Li, Chen Qin, Wenjia Bai, and Daniel Rueckert. Causality-inspired single-source domain generalization for medical image segmentation. *IEEE Transactions on Medical Imaging*, 2022.
19. Lv Tang, Haoke Xiao, and Bo Li. Can sam segment anything? when sam meets camouflaged object detection. *arXiv preprint arXiv:2304.04709*, 2023.
20. Tao Yu, Runseng Feng, Ruoyu Feng, Jinming Liu, Xin Jin, Wenjun Zeng, and Zhibo Chen. Inpaint anything: Segment anything meets image inpainting. *arXiv preprint arXiv:2304.06790*, 2023.
21. QiuHong Shen, Xingyi Yang, and Xinchao Wang. Anything-3d: Towards single-view anything reconstruction in the wild. *arXiv preprint arXiv:2304.10261*, 2023.
22. Jinyu Yang, Mingqi Gao, Zhe Li, Shang Gao, Fangjing Wang, and Feng Zheng. Track anything: Segment anything meets videos. *arXiv preprint arXiv:2304.11968*, 2023.
23. Jiazhong Cen, Zanwei Zhou, Jiemin Fang, Wei Shen, Lingxi Xie, Xiaopeng Zhang, and Qi Tian. Segment anything in 3d with nerfs. *arXiv preprint arXiv:2304.12308*, 2023.
24. Defeng Xie, Ruichen Wang, Jian Ma, Chen Chen, Haonan Lu, Dong Yang, Fobo Shi, and Xiaodong Lin. Edit everything: A text-guided generative system for images editing. *arXiv preprint arXiv:2304.14006*, 2023.
25. Teng Wang, Jinrui Zhang, Junjie Fei, Yixiao Ge, Hao Zheng, Yunlong Tang, Zhe Li, Mingqi Gao, Shanshan Zhao, Ying Shan, et al. Caption anything: Interactive image description with diverse multimodal controls. *arXiv preprint arXiv:2305.02677*, 2023.

26. Renrui Zhang, Zhengkai Jiang, Ziyu Guo, Shilin Yan, Junting Pan, Hao Dong, Peng Gao, and Hongsheng Li. Personalize segment anything model with one shot. *arXiv preprint arXiv:2305.03048*, 2023.
27. Zhihe Lu, Zeyu Xiao, Jiawang Bai, Zhiwei Xiong, and Xinchao Wang. Can sam boost video super-resolution? *arXiv preprint arXiv:2305.06524*, 2023.
28. Yang Liu, Muzhi Zhu, Hengtao Li, Hao Chen, Xinlong Wang, and Chunhua Shen. Matcher: Segment anything with one shot using all-purpose feature matching. *arXiv preprint arXiv:2305.13310*, 2023.
29. Zeyu Xiao, Jiawang Bai, Zhihe Lu, and Zhiwei Xiong. A dive into sam prior in image restoration. *arXiv preprint arXiv:2305.13620*, 2023.
30. Jun Cen, Yizheng Wu, Kewei Wang, Xingyi Li, Jingkan Yang, Yixuan Pei, Lingdong Kong, Ziwei Liu, and Qifeng Chen. Sad: Segment any rgbd. *arXiv preprint arXiv:2305.14207*, 2023.
31. Ruining Deng, Can Cui, Quan Liu, Tianyuan Yao, Lucas W Remedios, Shunxing Bao, Bennett A Landman, Lee E Wheless, Lori A Coburn, Keith T Wilson, et al. Segment anything model (sam) for digital pathology: Assess zero-shot segmentation on whole slide imaging. *arXiv preprint arXiv:2304.04155*, 2023.
32. Saikat Roy, Tassilo Wald, Gregor Koehler, Maximilian R Rokuss, Nico Disch, Julius Holzschuh, David Zimmerer, and Klaus H Maier-Hein. Sam. md: Zero-shot medical image segmentation capabilities of the segment anything model. *arXiv preprint arXiv:2304.05396*, 2023.
33. Yihao Liu, Jiaming Zhang, Zhangcong She, Amir Kheradmand, and Mehran Armand. Samm (segment any medical model): A 3d slicer integration to sam. *arXiv preprint arXiv:2304.05622*, 2023.
34. Tao Zhou, Yizhe Zhang, Yi Zhou, Ye Wu, and Chen Gong. Can sam segment polyps? *arXiv preprint arXiv:2304.07583*, 2023.
35. Chuanfei Hu and Xinde Li. When sam meets medical images: An investigation of segment anything model (sam) on multi-phase liver tumor segmentation. *arXiv preprint arXiv:2304.08506*, 2023.
36. Sheng He, Rina Bao, Jingpeng Li, P Ellen Grant, and Yangming Ou. Accuracy of segment-anything model (sam) in medical image segmentation tasks. *arXiv preprint arXiv:2304.09324*, 2023.
37. Maciej A Mazurowski, Haoyu Dong, Hanxue Gu, Jichen Yang, Nicholas Konz, and Yixin Zhang. Segment anything model for medical image analysis: an experimental study. *arXiv preprint arXiv:2304.10517*, 2023.
38. Yizhe Zhang, Tao Zhou, Peixian Liang, and Danny Z Chen. Input augmentation with sam: Boosting medical image segmentation with segmentation foundation model. *arXiv preprint arXiv:2304.11332*, 2023.
39. Peilun Shi, Jianing Qiu, Sai Mu Dalike Abaxi, Hao Wei, Frank P-W Lo, and Wu Yuan. Generalist vision foundation models for medical imaging: A case study of segment anything model on zero-shot medical segmentation. *arXiv preprint arXiv:2304.12637*, 2023.
40. Mingzhe Hu, Yuheng Li, and Xiaofeng Yang. Skinsam: Empowering skin cancer segmentation with segment anything model. *arXiv preprint arXiv:2304.13973*, 2023.
41. Yuhao Huang, Xin Yang, Lian Liu, Han Zhou, Ao Chang, Xinrui Zhou, Rusi Chen, Junxuan Yu, Jiongquan Chen, Chaoyu Chen, et al. Segment anything model for medical images? *arXiv preprint arXiv:2304.14660*, 2023.
42. Dongjie Cheng, Ziyuan Qin, Zekun Jiang, Shaoting Zhang, Qicheng Lao, and Kang Li. Sam on medical images: A comprehensive study on three prompt modes. *arXiv preprint arXiv:2305.00035*, 2023.

43. Yichi Zhang and Rushi Jiao. How segment anything model (sam) boost medical image segmentation? *arXiv preprint arXiv:2305.03678*, 2023.
44. Jun Ma and Bo Wang. Segment anything in medical images. *arXiv preprint arXiv:2304.12306*, 2023.
45. Yuheng Li, Mingzhe Hu, and Xiaofeng Yang. Polyp-sam: Transfer sam for polyp segmentation. *arXiv preprint arXiv:2305.00293*, 2023.
46. Olaf Ronneberger, Philipp Fischer, and Thomas Brox. U-net: Convolutional networks for biomedical image segmentation. In *Medical Image Computing and Computer-Assisted Intervention–MICCAI 2015: 18th International Conference, Munich, Germany, October 5-9, 2015, Proceedings, Part III* 18, pages 234–241. Springer, 2015.
47. Ali Hatamizadeh, Yucheng Tang, Vishwesh Nath, Dong Yang, Andriy Myronenko, Bennett Landman, Holger R Roth, and Daguang Xu. Unetr: Transformers for 3d medical image segmentation. In *Proceedings of the IEEE/CVF winter conference on applications of computer vision*, pages 574–584, 2022.
48. Bloch N., Madabhushi A., Huisman H., Freymann J., et al. NCI-ISBI 2013 challenge: Automated segmentation of prostate structures, 2015. <https://www.cancerimagingarchive.net>.
49. Guillaume Lemaître, Robert Martí, Jordi Freixenet, Joan C Vilanova, Paul M Walker, and Fabrice Meriaudeau. Computer-aided detection and diagnosis for prostate cancer based on mono and multi-parametric mri: a review. *Computers in biology and medicine*, 60:8–31, 2015.
50. Geert Litjens, Robert Toth, Wendy van de Ven, Caroline Hoeks, Sjoerd Kerkstra, Bram van Ginneken, Graham Vincent, Gwenael Guillard, Neil Birbeck, Jindang Zhang, et al. Evaluation of prostate segmentation algorithms for mri: the promise12 challenge. *Medical image analysis*, 18(2):359–373, 2014.
51. Takeru Miyato, Shin-ichi Maeda, Masanori Koyama, and Shin Ishii. Virtual adversarial training: a regularization method for supervised and semi-supervised learning. *IEEE transactions on pattern analysis and machine intelligence*, 41(8):1979–1993, 2018.
52. Kaiyang Zhou, Yongxin Yang, Yu Qiao, and Tao Xiang. Domain generalization with mixstyle. In *International Conference on Learning Representations*, 2021.
53. Fabian Isensee, Paul F Jaeger, Simon AA Kohl, Jens Petersen, and Klaus H Maier-Hein. nnu-net: a self-configuring method for deep learning-based biomedical image segmentation. *Nature methods*, 18(2):203–211, 2021.